# Pump/Probe Spectroscopy of NaI in Rare Gas Environments: A Statistical Description

**H. Dietz and V. Engel***

*Institut für Physikalische Chemie, Universität Würzburg, Am Hubland, 97074 Würzburg, Germany*

*Received: April 16, 1998; In Final Form: June 29, 1998*

A theoretical study of the femtosecond spectroscopy of the NaI predissociation process under high-pressure conditions is presented. We employ a statistical model to mimic the pressure dependence of pump/probe signals for different rare gases. The model uses an ensemble of trajectories to approximate the quantum dynamics of the wave packet, which is prepared by ultrashort pulse excitation. Predissociation is treated within the Landau−Zener model for curve crossing. Collisions are modeled as instantaneous events assuming hard sphere scattering. The collision probability is calculated statistically so that no adjustable parameter has to be introduced. The results show how coherent wave packet motion is influenced by scattering processes and how this is reflected in femtosecond pump/probe signals.

## I. Introduction

The goal to observe chemical reactions that take place on the femtosecond time scale in real time has been achieved today. The pioneering work of Zewail and co-workers[1] and other research groups[2−5] provided us with insight into the kinetics of primary chemical reactions. Many reactions taking place in the gas phase and liquid surroundings have been studied using the techniques and ideas of femtochemistry.[6]

The predissociation of the NaI molecule has served as a textbook example to study many basic features of scattering,[7] high-resolution,[7,8] and time-resolved spectroscopy.[9] In particular, the electronic predissociation process that occurs after excitation from the ionic ground state to a first excited state has been studied in great detail in the time domain. Here, e.g., nonlinear transient effects,[10] the control of chemical reactions,[11] and the long-time behavior of wave packet motion[12] have been studied.

Whereas the above-mentioned experiments were conducted under gas-phase conditions, more recent investigations examined the influence of high-pressure rare gas environments on the pump/probe signals for the NaI predissociation.[13] Similar work has been performed before by Zewail and co-workers, who studied the dissociation and caging dynamics of iodine in rare-gas solvents in the gas-to-liquid region.[14−16]

From a theoretical point of view, the correct treatment of such processes is rather demanding. Ideally one should describe the molecule that is observed in the experiment by the use of a reduced density matrix description.[17] One also might use approximative quantum or mixed quantum/classical descriptions.[18] For some recent work with applications to molecular systems, see, e.g., ref 19. Yet another approach is to perform a full molecular dynamics simulation. Such calculations have been performed simulating wave packet dynamics in various surroundings.[20−22] In the work of Apkarian, Martens, and co-workers,[20] the wave packet that is prepared by femtosecond excitation is represented by many classical trajectories. The present work follows this approach to describe the pump/probe spectroscopy of NaI under high-pressure conditions: the wave packet motion in the coupled electronic states of NaI is approximated by bundles of classical trajectories. However, we use a simpler method and do not explicitly solve the equations of motion for the colliding atoms. This model was applied before to some aspects of the NaI predissociation under collision conditions,[23] and the experimental results[13] could be explained. Here we present a full account of such dynamical processes.

The paper is organized as follows: section II describes a statistical model to monitor the wave packet dynamics, the influence of collisions, and the calculation of pump/probe signals. In section III we study the NaI−Ar system. Collisions with other rare gas atoms are treated in section IV. The final section V contains a summary of the paper and gives an outlook to other applications.

## II. Theory

We regard femtosecond excitation of NaI from its electronic ground $|0\rangle$ to the excited state $|1\rangle$ (the $\Omega^+$ state). These states of alike symmetry show an avoided crossing at a bond length of 6.9 Å. Figure 1 illustrates the excitation scheme. The plot indicates the center wavelength of a pump and a time-delayed probe pulse. Under collision-free conditions the first pulse prepares a wave packet at the inner potential wall of the excited-state potential. The packet moves outward until the region where the nonadiabatic coupling between the ground and excited state is effective is reached. Then, the packet splits into a component that moves into the asymptotic region (representing the fraction of dissociated NaI molecules) and another one that stays bound and is reflected at the outer turning point to return into the inner potential region.

The motion of the wave packet is probed by excitation to an excited electronic state $|2\rangle$ which decays via fluorescence. The total fluorescence signal is proportional to the population in state $|2\rangle$ prepared by the interaction of the sample with the pump and probe pulse. An efficient population transfer $|2\rangle \leftarrow |1\rangle$ takes place if the wave packet in state $|1\rangle$ is located in the Franck−Condon window that depends on the probe excitation wavelength. In our case this window is located left of the crossing point region so that the detection monitors the decay of the quasi-bound molecule.[9]

Our aim is to describe pump/probe signals that are influenced by collisions with rare gas atoms. Instead of performing a full molecular dynamics simulation or full quantum calculations,

S1089-5639(98)01890-8 CCC: $15.00 
Published on Web 08/29/1998

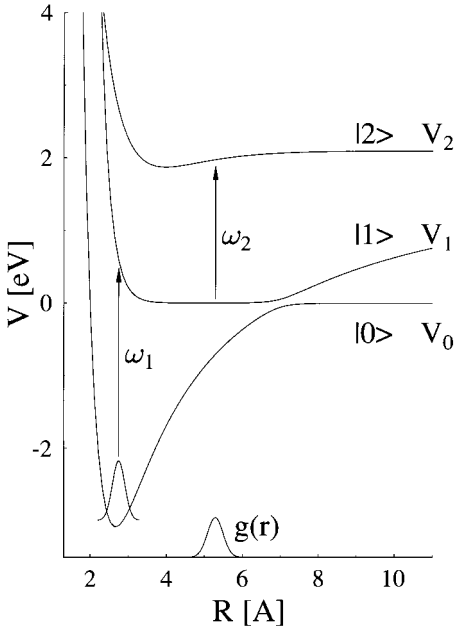


**Figure 1.** NaI pump/probe excitation scheme. The center frequencies of pump and probe pulse are indicated as vertical arrows. The Franck−Condon window for the probe transition is marked on the horizontal axis and the initial vibrational state is shown schematically.

we will develop a statistical model that uses bundles of classical trajectories to describe the NaI dynamics but does not explicitly treat the NaI−rare gas collisions by solving the classical equations of motion for the combined system; rather collisions take place as instantaneous processes.

**II.A. Unperturbed Motion.** Quantum mechanically we may calculate the function prepared in the pump process by using first-order time-dependent perturbation theory. The nuclear wave function in the upper state (denoted as $|1\rangle$ in what follows) can be written as (atomic units are employed throughout)

$$\psi_1(R, t) = \frac{1}{i}\int_{-\infty}^{t} \mathrm{d}t'\, U_1(t-t')\, W_{10}(t')\, U_0(t')\, \psi_0(R) \quad (1)$$

where $R$ is the bond length. $\psi_0(R)$ is the initial vibrational state in the electronic ground state $|0\rangle$. $U_n$ are the propagators in the two states, and the molecule-field interaction $W_{10}(t)$ describing the absorption process is given by

$$W_{10}(t) = -\frac{1}{2}\mu_{10} f_1(t) e^{-i\omega_1 t} \quad (2)$$

Here $\mu_{10}$ is the projection of the transition dipole moment on the laser polarization vector. The laser pulse is characterized by its envelope function $f_1(t)$ and frequency $\omega_1$.

In our model the quantum dynamics of this wave function is represented by a set of classical trajectories $R_n(t)$, which are chosen to represent the quantum mechanical probability distribution. We assume a Gaussian envelope function for the pump pulse so that its spectral width defines a Gaussian energy distribution peaked at the energy corresponding to $\omega_1$. According to the time and frequency distribution of the pulse, we sample at random times $t_n$ and energies $\epsilon_n$. Trajectories are started at times $t_n$ with zero momentum at the inner classical turning point where $V_1 = \epsilon_n$. Within this method the classical counterpart of eq 1 is

$$\rho_1^{\mathrm{cl}}(R, t) = \frac{1}{N}\sum_{n=1}^{N} R_n(t) \quad (3)$$

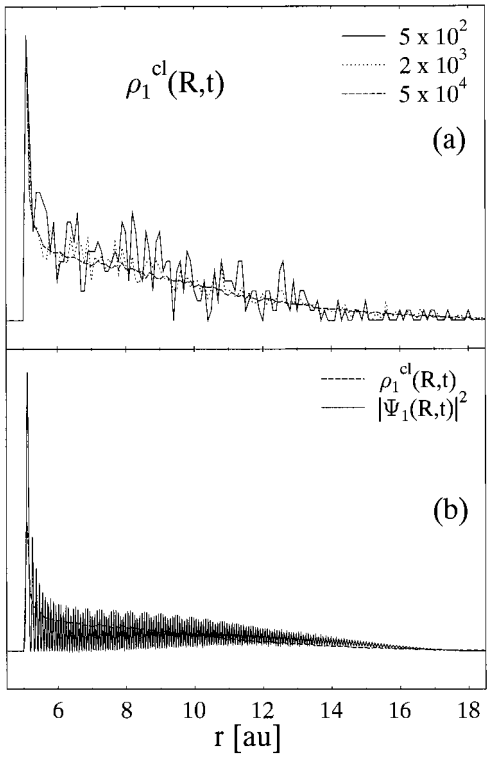


**Figure 2.** (a) Classical trajectory distribution $\rho_1^{cl}(R, t)$ (eq 3) at time $t = 4.2$ ps, calculated for different numbers $N$ of trajectories, as indicated. (b) The modulus squared of the quantum mechanical wave function (eq 1) is compared to $\rho_1^{cl}(R, t)$.

where $R_n(t)$ are the trajectories with the initial conditions as specified above. We emphasize that our trajectories are sampled from a two-dimensional distribution, which is a function of energy and time. This distribution is fixed by the properties of the pump pulse, i.e., its time and frequency dependence. Another possibility, which is most commonly employed in classical simulations of quantum dynamics, is a sampling of the Wigner function[24] calculated from the ground-state vibrational wave function. In both cases the sampling is performed over initial conditions for coordinates and momenta. In this sense both approaches, which are after all only recipes, are equivalent. Our approach, which gives very good agreement with quantum mechanics (see below), is somehow simpler and does not have the problem that the sample function can become negative like it is found for the Wigner function.[24]

In Figure 2 we compare the quantum to the classical dynamics. Here the predissociation channel was disregarded so that we treat dynamics in the upper adiabatic well exclusively. The wave packet was calculated as described in ref 25 and propagated with the split-operator method.[26] Figure 2a shows the coordinate distribution of the weighted trajectories at a time of 4.2 ps for 500, 2000, and 50 000 sample points, respectively. As expected, the curves become smoother with increasing number of points. The deviation between the results for 2000 and 50 000 points are actually rather small so that the statistics converges fast.

Figure 2b compares the highly oscillatory quantum mechanical wave function with the classical trajectory swarm. The normalization was chosen such that $\int \mathrm{d}R \rho_1^{\mathrm{cl}}(R, t) = \int \mathrm{d}R |\psi_1(R, t)|^2 = 1$. The envelope of the quantum probability distribution is astonishingly well reproduced. We not that the functions are shown for a time after four vibrational periods taking place in an extremely anharmonic potential. Calculating the expectation value of $R$ we find 9.23 au in the quantum

mechanical and 8.52 in the classical case, which is a very good agreement taking the large extent of the wave function into account. Furthermore, the wave function displayed in Figure 2b is already the worst case in the sense that standing wave features are found that cannot by any means be represented by a distribution of classical trajectories. Overall, the results strengthen our assumption that we might simulate the pump/probe experiments classically as was shown before in other cases.[27]

The fluorescence signal for pump/probe excitation at time $T$ is proportional to the population $I_2(T)$ created by the probe pulse in state $|2\rangle$. In the Appendix it is shown that the pump/probe signal can be approximated by the expression

$$I(T) = \frac{1}{N}\sum_{n=1}^{N}\int_{-\infty}^{\infty} \mathrm{d}t\, f(\sqrt{2}(t-T))\, F(D(R_n(t-T)) - \omega_2) \qquad (4)$$

Here $D(R_n(t))$ is the difference $V_2 - V_1$ between the potentials of the states $|2\rangle$ and $|1\rangle$, calculated at the position of the $n$th trajectory at time $t$. $F(D(R_n(t)) - \omega_2)$ is the Fourier transform of the pulse envelope function with respect to the argument $D(R_n(t)) - \omega_2$. Similar expressions for the pump/probe signal have been used before in numerical simulations.[20] For a derivation using the semiclassical limit of the Liouville formalism, see ref 28.

Let us next turn to molecular collisions.

**II.B. AB + C Collisions.** In what follows we regard only quasi-collinear collisions in which rare gas atoms can collide either from the Na or I side of the diatomic molecule. This means that the momenta of Na (or I) and the incoming atom are parallel to each other. Let us describe a general AB + C collision, so that C collides with atom B only. The calculation of the pump/probe signal within our statistical model proceeds as follows:

1. A trajectory $R_n(t)$ is chosen to describe the relative motion of AB.

2. The center of mass momentum $p_{AB}$ of the molecule AB and the momentum $p_C$ of the atom C are chosen via Monte Carlo sampling from a Maxwell−Boltzmann distribution reflecting the experimental conditions.

3. The collision probability $P_{sc}$ at time $\Delta t$ is assumed to be proportional to the time interval $\Delta t$, the relative velocity $v_{BC}$ between the atoms B and C, the hard sphere cross section $\sigma = \pi(r_B + r_C)^2$, and the density of C atoms. Since in the experiments to be described the AB density is negligible compared to the C density, AB−AB collisions are neglected.

4. We calculate the collision probability $P_{sc}$ at each time step. If a negative probability is found (which happens for negative relative velocities of the collision partners), the trajectory is integrated for another time step without any modifications. For positive probability we choose a random number $s$ from the unit interval and if $P_{sc} < s$ the trajectory is integrated for the next time step.

5. In the case $P_{sc} > s$ the momentum transfer along the internuclear axis of the molecule, $(P_B, P_C) \rightarrow (P'_B, P'_C)$, is calculated in the rest frame of the (B, C) center of mass. To this end the impact parameter $b$ is chosen at random according to the distribution $f(b)\,\mathrm{d}b = b/\sigma$. A brief and simple calculation shows that the momentum transfer is uniformly distributed in the interval $[0, \Delta p_{max}]$, where the maximal momentum transfer $\Delta p_{max}$ is obtained in the case of a central collision. The perpendicular component of the momentum transfer is ignored. Hence our model overestimates the energy loss in the NaI internal motion by ignoring rotational excitation.

6. The trajectory is integrated further in time with the new kinetic energy calculated from the energy transfer during the collision.

7. If the crossing point between the two potential curves is passed during a time step, the hopping probability is calculated using the Landau−Zener formula[29]

$$P_{LZ} = e^{-(2\mu)^{1/2}F/v_{BC}} \qquad (5)$$

where $\mu$ is the reduced mass of BC and in our case $F = 0.503$ au. A random number $s_h$ is taken from the unit interval, and if $P_{LZ} > s_h$ the potential curve is changed and the integration for the next step is performed on this potential.

8. The signal is calculated according to eq 4.

The generalization to treat AB + C and C + AB collisions simultaneously is straightforward. In the above point 4, the collision probabilities for both collisions are calculated. If both are larger than the random number, both collisions occur simultaneously and the change in velocity of both atoms A, B is taken into account.

We now turn to the numerical results obtained from our statistical model in describing the pump/probe spectroscopy of NaI in various rare gas environments.

## III. The NaI−Ar System

In what follows we will describe NaI molecules that are excited with ultrashort laser pulses and afterward collide with Ar atoms under different experimental conditions. We will regard two situations where in the first case the motion in the excited electronic state is probed and in the second case the dynamics in the lowest adiabatic, i.e., the ground electronic state, is probed.

**III.A. Excited-State Dynamics.** In this section we regard NaI−Ar collisions under different pressure conditions. The temperature is set to 960 K as it was fixed in recent experiments.[13] The pump pulse has a width of 50 fs and a center wavelength of 320 nm. For the probe pulse the same width was taken but the wavelength was 620 nm. The Franck−Condon window for the probe transition, where the excitation probability is maximal, is located at distances shorter than the crossing point region and is marked in Figure 1. We sampled $10^4$ initial trajectories to calculate the pump/probe signals that are displayed in Figure 3. The pressure enters in our calculation through the Ar density, which appears in the formula for the collision probability. The Ar density is related to the pressure via the ideal gas equation. To calculate the hard sphere cross section we used Lennard-Jones radii taken from ref 30 for $Na^+$ and $I^-$ ions. Since these numbers may slightly differ from the "best" hard sphere radii, the numbers given for the pressure are not to be seen as extremely accurate.

For zero pressure a signal is obtained that reflects the quasi-bound motion of the wave packet $\psi_1$[9,31] (Figure 3, upper panel). The doublet in the single peaks appears since the packet passes the Franck−Condon window on its way in- and outward.[32,31] With increasing pressure, the periodic signal that occurs for 0 bar pressure is destroyed earlier and an increasing background arises. The strong modification of the signal through the collision processes has to be anticipated, but let us analyze the behavior of the signals more carefully.

The first observation is the occurrence of a peak around 0.7 ps that appears clearly for pressures above 210 bar. The height of the peak rises with increasing pressure. This feature is due to trajectories that have undergone collisions. Upon a collision the NaI relative motion loses energy, which reduces the classical

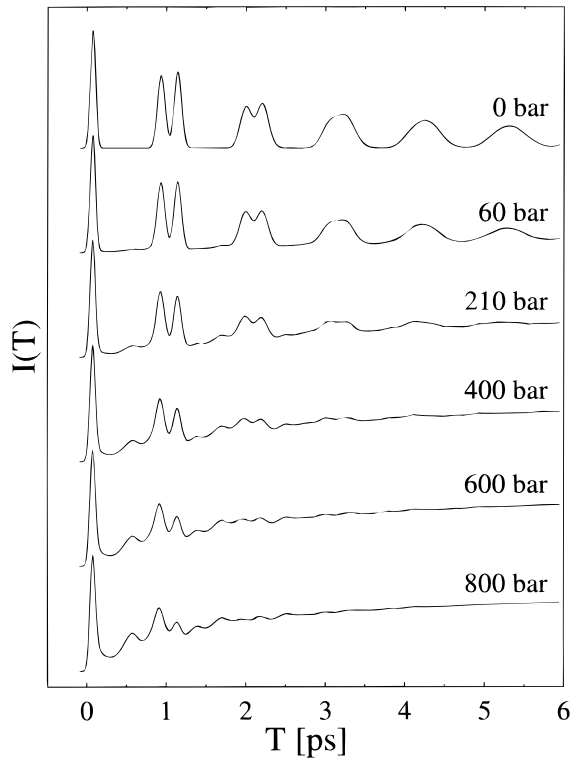


**Figure 3.** NaI−Ar collisions. Pump/probe signals detecting the excited-state dynamics are shown for different Ar pressures. The uppermost curve corresponds to the unperturbed NaI motion.

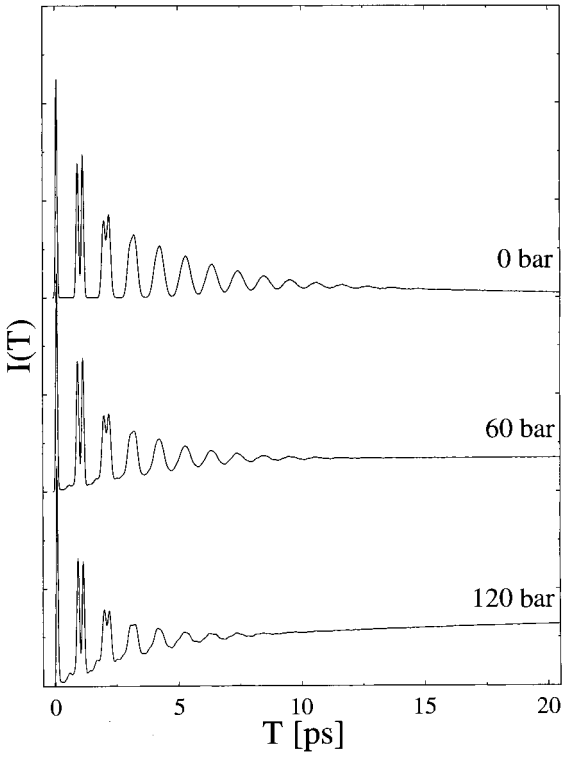


**Figure 4.** Same as Figure 3 but for longer delay-times.

period so that the classical orbits return to the Franck−Condon window much earlier. A calculation shows that over a large energy interval (for energies in the range between 0.15 and 0.55 eV) the classical period remains almost constant at a value of about 0.8 ps. This means that the position of the peak does not change essentially over a broad distribution of pressures.

The behavior of the signal for long delay times and for different pressures is quite interesting. As a trend we notice that the intensity of the asymptotic signal increases relative to the height of the first peak around zero delay times, which is the same under all pressure conditions regarded here. The underlying process is a collisional stabilization since it means that less NaI molecules predissociate with increasing collision probability. It is easy to rationalize that under high-pressure conditions the NaI relative motion is relaxed toward lower total energy. As a consequence the Landau−Zener probability (eq 5) for dissociation is reduced. Thus, through a loss of energy during the scattering process the NaI molecules are more stable than under collision-free conditions. The effect can be seen more clearly in the long-time behavior of the pump/probe signal as displayed in Figure 4. Curves are shown for a time interval ranging up to 20 ps and for three different pressures, as indicated. The asymptotic signal, reflecting the number of molecules that are still bound, shows that with increasing pressure more molecules remain bound and thus do not predissociate.

As a complementary information we might look at the population of the fragment channel and calculate the fraction of the total number of trajectories that enter the asymptotic region through the hopping process as a function of time. Curves for different pressures are displayed in Figure 5. Collisions of free Na or I atoms with Ar are not regarded here. The characteristic step functions, as detected in the zero pressure case,[9,31] show a sudden increase of fragment population each

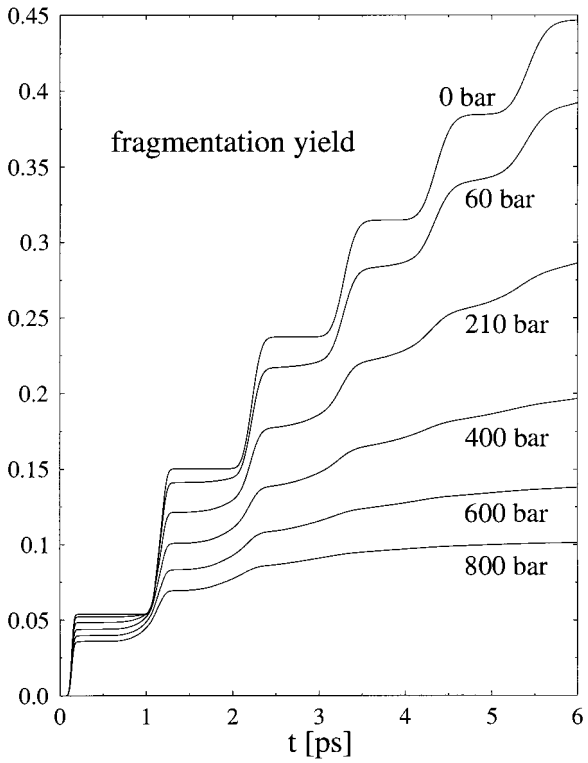


**Figure 5.** NaI−Ar collisions: fragmentation yield of NaI as a function of time for different pressures, as indicated.

time the wave packet passes the crossing point region on its way outside. The height of the steps directly reflects the nonadiabatic coupling strength. An increase in pressure increases the efficiency of the energy loss process so that the NaI molecules become more stable with respect to dissociation. This is demonstrated most dramatically in the case of 800 bar pressure where less than 10% of the molecules are found in the fragmentation channel at long times. To understand the energy-

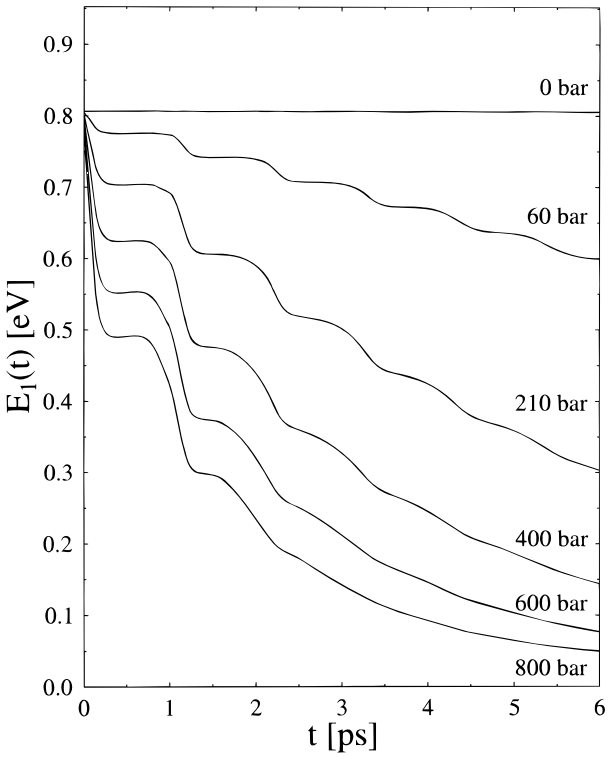


**Figure 6.** Energy relaxation induced by Ar collisions in the excited electronic state of NaI. The mean energy $E_1(t)$ (eq 6) is shown for times up to 6 ps.

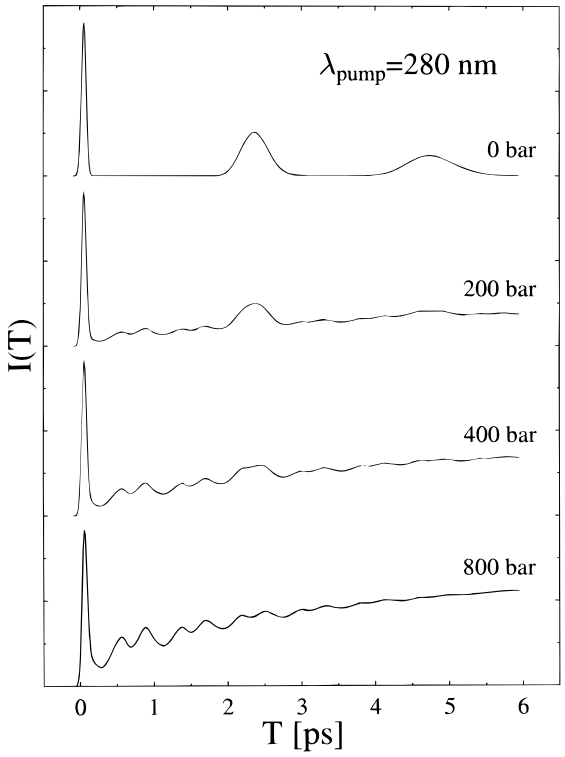


**Figure 7.** Pump/probe signals for the excited-state dynamics at different Ar pressures and a pump wavelength of 280 nm.

transfer process in more detail we calculate the mean energy of the bound excited NaI molecules defined as

$$E_1(t) = \frac{1}{N_1}\sum_n H_1(R_n(t)) \qquad (6)$$

where $H_1$ is the classical Hamilton function corresponding to the excited electronic state and $N_1$ is the number of trajectories in this state.

Figure 6 displays $E_1(t)$, calculated under different pressure conditions. In the zero pressure limit a constant curve at a value slightly less than 0.81 eV, which corresponds to the mean energy of a wave packet prepared by a 320 nm excitation, is found. Already at 60 bar pressure the energy loss process is quite efficient. The curve shows that the energy transfer takes place at certain time intervals only, which is due to our assumption that the collision probability is proportional to the relative velocity of the Ar atom and its collision partner so that as long as the bond length increases rapidly the collision probability is large. The trend which can be taken from the curves is that with increasing pressure the energy transfer takes place earlier and is more efficient. In the case of 800 bar the total energy of NaI after 5 ps is less than 10% compared to the initial energy. Since in this case the total energy is rather small for long times, the relative motion of the atoms in the molecule with respect to the argon atom does not differ very much during in- and outward motion in the molecule, which has the consequence that the distinct steps disappear in the $E_1(t)$ curve. Another reason for this behavior is the occurrence of multiple collisions, which cause the trajectories to move out of phase.

Let us next discuss the signal obtained for a pump excitation wavelength of 280 nm. In this case, the mean initial energy of the moving wave packet is much higher and the vibrational period is about 2.4 ps, as can be seen in the zero pressure curve in Figure 7. Since the mean peaks now are well-separated, the additional structures appearing at higher pressures can be seen far more clearly compared to the 320 nm case displayed in Figure 3. With increasing wavelength the peaks due to collisions shift in the vicinity of the peak that stems from the unperturbed motion, and it will be difficult to separate them experimentally. As a consequence we conclude that the effect of the collisions are better studied for lower excitation wavelengths.

Finally we note that in the NaI−Ar collision system the temperature dependence of the pump/probe signals is not dramatic as long as the density of the rare gas atoms is kept constant. This comes about since the kinetic energy of the relative motion in NaI is so much higher than the kinetic energy of the thermal motion of argon (1 eV compared to 0.1 eV at 960 K).

**III.B. Ground-State Dynamics.** In the previous section we considered the wave packet motion in the upper adiabatic state displayed in Figure 1. The total wave function has a second component that belongs to the lower adiabatic state of the problem. The dynamics of this nuclear component and its modification through collisions will be discussed in what follows. We note that in order to get converged results about $10^5$ trajectories have to be used in the simulation. This is an order of magnitude larger than in the case of the excited-state dynamics since only a small fraction of trajectories enter the ground state. To monitor the motion we use a probe pulse of 470 nm and assume a direct transition $|2\rangle \leftarrow |0\rangle$. For this wavelength, the Franck−Condon window is the same as used in section III.A, i.e., the one that is marked in Figure 1. Signals obtained under different pressure conditions are displayed in Figure 8. In the unperturbed case the quasibound vibrational motion is seen in the plot. Also, at longer times the noise on the curves shows that the statistics is still not good enough. Compared to the excited-state dynamics (Figure 3), we observe that the first peak around 1 ps is missing in the signal since the first time the ground-state wave packet reaches the probe

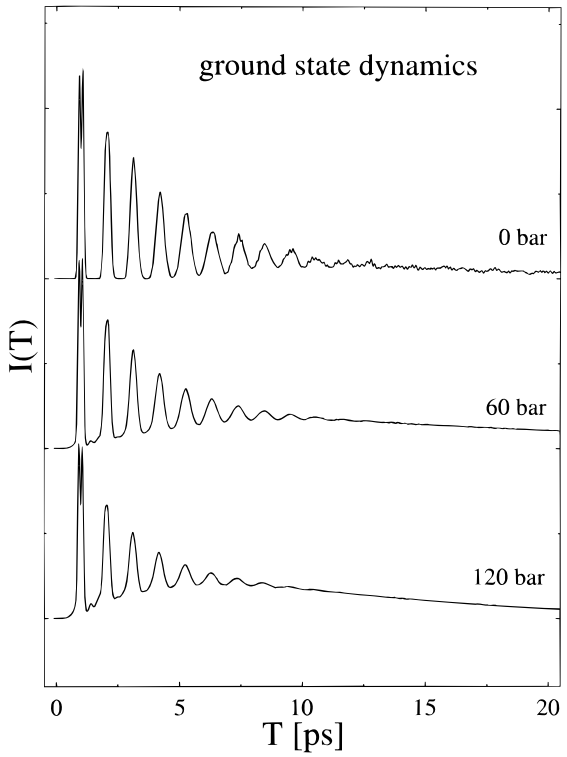


**Figure 8.** Pump/probe signals detecting the ground-state dynamics of NaI at different Ar pressures.

window occurs after the curve crossing on the way inward. The collision processes now have a different effect on the signal: with increasing pressure the asymptotic signals decrease, contrary to what is found for the probe of the excited-state dynamics. The periodic behavior stems from the returning wave packet in the upper state; i.e., the population in the ground state is increased during the passing of this high-energy component. The collisions now have two effects. First, the dissociation channel is closed through energy loss in the excited state (see section III.A). Thus there is no longer a population transfer to the ground state. Second, the collisions induce an effective vibrational relaxation in the electronic ground state so that the corresponding trajectories become trapped. Since much energy is transferred from the molecule to the colliding atoms, the vibrational energy decreases and the probe window is no longer reached by the trajectories so that the periodicity is lost and the signal approaches zero. A calculation of the mean classical energy $E_0(t)$ (eq 6 for the classical Hamilton function $H_0$ of the ground state) shows that with increasing pressure more and more energy is lost and, for 800 bar, the sample of molecules approaches thermal equilibrium in the ground state.

In summary we conclude that an observation of the ground-state component of the total wave function yields information about the vibrational energy relaxation and thus gives hints about the nature of the energy-transfer processes between the predissociating molecules and the surrounding atoms.

## IV. NaI−X (X = He, Xe) Collisions

Let us now regard other noble gases as collision partners with the NaI molecule. Within our model two modifications have to be made if the atomic collision partners are replaced: besides the different mass the initial momenta of the noble gas atoms have to be replaced. Furthermore the hard sphere cross section that enters into the collision probability changes.[30]

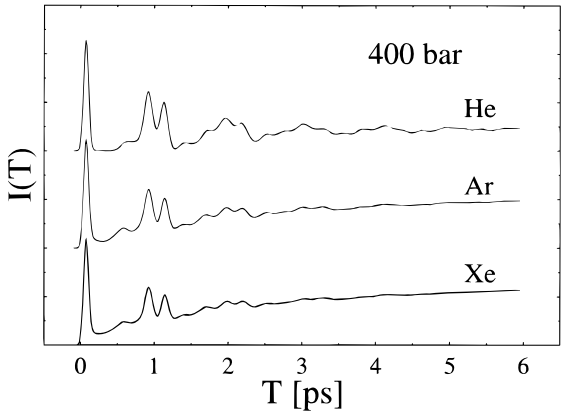


**Figure 9.** Comparison of pump/probe signals for collisions with different rare gas atoms. The signals belong to the excited-state dynamics at a pressure of 400 bar.

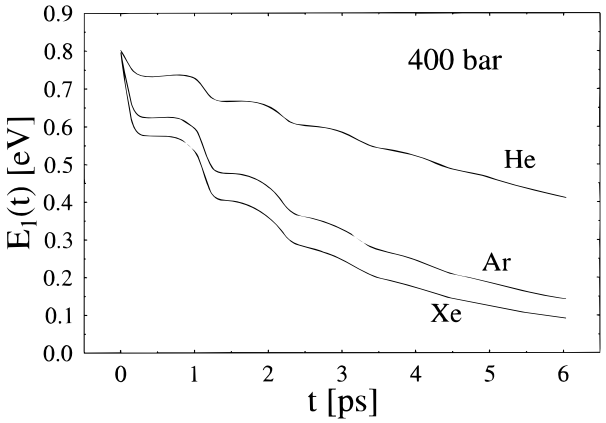


**Figure 10.** Mean energy of NaI in its excited electronic state (eq 6) for different rare gas collision partners.

Figure 9 compares pump/probe signals for He, Ar, and Xe collisions at 400 bar pressure. Here we consider probe signals resulting from the excited-state dynamics. At a first glance the curves are very similar. In particular the peaks in the signals occur at the same times and are of similar shape. A closer look, however, shows that with increasing mass of the rare gas atoms the asymptotic signal increases. This can be understood by analyzing the time evolution of the mean energy $E_1(t)$ of the bound NaI complex. This function is shown in Figure 10. Clearly, the energy relaxation due to the collisions is more effective for heavier rare gas atoms. As a consequence the stabilization effect that stems from a blocking of the dissociation channel for small energy (see section III.A) is of minor significance in the helium case. Thus the magnitude of the long-time signal is a direct measurement of the averaged energy transfer taking place in the collision processes. On the other hand, the curves show that the mere effect of the collisions is that the trajectories describing the NaI wave packet motion are influenced to get out of phase so that additional structures in the pump/probe signals occur. For other pressures similar trends are observed.

## V. Summary and Outlook

We have presented a detailed numerical study of the NaI predissociation process, which is initiated by femtosecond pulses and is influenced by collisions with rare gas atoms. The calculations combine classical and statistical methods and do not use any adjustable parameter. Samples of classical trajectories are used to represent the quantum mechanical wave

packet, which is prepared through femtosecond excitation in the NaI molecule. These trajectories are influenced by collisions with surrounding rare gas atoms. The scattering process is treated to occur statistically and with the hard sphere cross section. In this way no classical trajectories for the environment have to be integrated. Of course this model neglects the possible change of the potential curves of NaI due to the interaction with the rare gas atoms. This especially might change the Franck−Condon window for the probe transition. We expect the influence on the neutral−neutral transition that detects the dynamics in $|1\rangle$ to be rather small whereas the transition from the ionic ground state $|0\rangle$ is certainly more sensitive to the three-body interaction.

The excited NaI molecule loses energy of the relative motion in the collision processes. This vibrational relaxation yields two observable effects. First, the vibrational period of some molecules becomes smaller so that additional structures appear in the pump/probe spectra compared to the signal obtained in the unperturbed case. As a consequence, the coherent signal is washed out and the periodicities are lost for longer times. Second, since the dissociation probability decreases with decreasing energy the molecules become more stable with respect to fragmentation. For longer wavelengths of the pump pulse, where the vibrational period of the quasi-bound motion is longer, the effects of the collisions can be resolved more clearly. Whereas this effect is pronounced, the change of the temperature for fixed pressure does not result in any visible effect in the pump/probe signals. The quantum dynamics in the electronic ground state for high pressure is also strongly influenced by vibrational relaxation processes. For high enough pressures the system approaches thermal equilibrium, and a signal that detects vibrational motion in high vibrational states vanishes accordingly. Results for different rare gas environments show that a rather similar behavior of time-resolved fluoresesence signals is to be expected. Although the average energy transfer in NaI−He collisions is less than what is found in the NaI−Xe case, the signals for the two cases differ mainly in their asymptotic behavior.

Here we did not consider recombination processes. Within the present quasi-one-dimensional model these events will take place at some point. Here an extension of the theoretical description is necessary. Work in this direction is in progress.[34]

We believe that the approach presented here to treat collision processes between atoms and molecules prepared by coherent femtosecond excitation offers a valuable tool to achieve an insight into these dynamical process.

**Acknowledgment.** Financial support by the DFG within the Schwerpunktsprogramm "Time-Dependent Phenomena and Methods in Quantumsystems of Physics and Chemistry" and by the Fonds der Chemischen Industrie is gratefully acknowledged. We thank W. Kiefer, G. Knopp, A. Materny, and M. Schmitt for helpful discussions.

## Appendix

In what follows we derive the expression for the pump/probe signal $I_2(T)$ as used in our simulation.

The fluorescence signal for pump/probe excitation at time $T$ is proportional to the population in state $|2\rangle$, which is (within first-order perturbation theory)

$$P_2(T) = \langle\psi_2(T)|\psi_2(T)\rangle = \int_{-T}^{T} dt \int_{-T}^{T} dt' \, \langle\psi(_1-T)|U_1^{\dagger}(t+T)\, W_{21}^{*}(t)\, U_2(t-t')\, W_{21}^{*}(t')\, U_1(t'+T)|\psi_1(-T)\rangle \quad (7)$$

The interaction energy here is

$$W_{21}(t) = -\frac{1}{2}\mu_{21} e^{-i\omega_2 t} f(t) \quad (8)$$

with the same notation as used in section II. In what follows we assume the Condon approximation so that $\mu_{21}$ is a constant. Introducing the difference potential $D = V_2 - V_1$, eq 7 may be written as

$$I_2(T) = \int_{-T}^{T} dt \int_{-T}^{T} dt' \, W_{21}^{*}(t) \times W_{21}(t')\langle\psi_2(0)|U^{\dagger}{}_1(t)e^{-i(H_1+D)(t-t')}U_1(t')|\psi_1(0)\rangle \quad (9)$$

Here we shifted the time origin to the center of the pulse, i.e., the delay time $T$. To a first approximation we may neglect the commutator $[H_1, D]$, which results in the expression

$$\langle\psi_2(T)|\psi_2(T)\rangle \sim \int dR \, |F(D(R) - \omega_2)|^2 |\psi_1(0)|^2 \quad (10)$$

where we used the Fourier transform

$$F(D(R) - \omega_2) = \int_{-T}^{T} dt \, f(t) e^{i(D(R)-\omega_2)t} \quad (11)$$

and dropped all constants. The above expression is very useful since the excitation process does not have to be treated explicitly: the signal is proportional to the norm of the initial state at the pulse center, multiplied with a coordinate-dependent weight function.[35] The approximation does not account for the motion of the wave packet $\psi_1$ during the excitation process. This effect can be accounted for by extending the above approximation. In doing so we perform a splitting of the exponential operator containing $H_1 + D$

$$e^{-iH_1(t-t')-iD(t-t')} \sim e^{-iH_1(t-t')/2} e^{-iD(t-t')} e^{-iH_1(t-t')/2} \quad (12)$$

which is correct up to second order.[36] Inserting this splitting into eq 9 yields

$$I_2(T) = \int_{-T}^{T} dt \int_{-T}^{T} dt' \, W_{21}^{*}(t) \times W_{21}(t') \left\langle \psi_1\left(\frac{t+t'}{2}\right)\middle| e^{-iD(t-t')} \middle|\psi_1\left(\frac{t+t'}{2}\right)\right\rangle \quad (13)$$

A change of the variables ($t_1 = (t + t')/2$, $t_2 = t - t'$) yields the population

$$I_2(T) = \int_{-T}^{T} dt_1 \int_{-T}^{T} dt_2 \, f^{*}\left(t_1 + \frac{t_2}{2}\right) f\left(t_1 - \frac{t_2}{2}\right) \times \langle\psi_1(t_1)|e^{-i(D-\omega_2)t_2}|\psi_1(t_1)\rangle \quad (14)$$

In our simulation we assume Gaussian pulses of the form

$$f(t) = e^{-t^2/(2\sigma^2)} \quad (15)$$

which have the property

$$f\left(t_1 + \frac{t_2}{2}\right) f\left(t_1 - \frac{t_2}{2}\right) = f(\sqrt{2}t_1) f\left(\frac{t_2}{\sqrt{2}}\right) \quad (16)$$

Since the pulse is of finite length, we may extend the limits of the integrals to infinity so that the integration over $t_2$ may be performed as

$$\tilde{F}(D(R) - \omega_2) = \int_{-\infty}^{\infty} dt_2 \, e^{i(D(R)-\omega_2)t_2} f\left(\frac{t_2}{\sqrt{2}}\right) \quad (17)$$

Finally, the pump/probe signal at delay time $T$ takes the form

$$I(T) = \int_{-\infty}^{\infty} \mathrm{d}t\, f(\sqrt{2}t) \int \mathrm{d}R |\psi_1(t)|^2\, \tilde{F}(D(R) - \omega_2) \quad (18)$$

A comparison of this formula to the lower order approximation ref 9 shows that the wave packet motion of $\psi_1$ is included by a temporal average over its motion during the excitation process. We note that eq 18 represents the best approximation to the signal that does not need phase information.

The pump/probe signal calculated with the classical trajectories now is obtained as

$$I(T) = \frac{1}{N}\sum_{n=1}^{N} \int_{-\infty}^{\infty} \mathrm{d}t\, f(\sqrt{2}(t - T))\, \tilde{F}(D(R_n(t - T)) - \omega_2) \quad (19)$$

where the time origin was shifted back to $t = 0$.

## References and Notes


(1) Zewail, A. H. *Femtochemistry;* World Scientific: Singapore, 1994; Vols. 1 and 2.

(2) *J. Phys. Chem.* **1993**, *97*, Femtochemistry Special Issue.

(3) Chergui, M., Ed. *Femtochemistry*; World Scientific: Singapore, 1996.

(4) Sundström, V., Ed. *Femtochemistry and Femtobiology*; World Scientific: Singapore, 1997.

(5) *J. Phys. Chem. A* **1988**, Femtochemistry. Special Issue.

(6) Manz, J., Wöste, L., Eds. *Femtosecond Chemistry*; VCH: Weinheim, 1995.

(7) Berry, R. S. In *Alkali halide vapors*; Davidovits, P., McFadden, D. L., Eds.; Academic Press: New York, 1979.

(8) Schaefer, S. H.; Bender, D.; Tiemann, E. *Chem. Phys.* **1982**, *92*, 273. Schaefer, S. H.; Bender, D.; Tiemann, E. *Chem. Phys. Lett.* **1984**, *89*, 65.

(9) Rose, T. S.; Rosker, M. J.; Zewail, A. H. *J. Chem. Phys.* **1988**, *88*, 6672. Rosker, M. J.; Rose, T. S.; Zewail, A. H. *Chem. Phys. Lett.* **1988**, *146*, 175. Rose, T. S.; Rosker, M. J.; Zewail, A. H. *J. Chem. Phys.* **1989**, *91*, 7415.

(10) Materny, A.; Herek, J. L.; Cong, P.; Zewail, A. H. *J. Phys. Chem.* **1994**, *98*, 3352.

(11) Herek, J. L.; Materny, A.; Zewail, A. H. *Chem. Phys. Lett.* **1994**, *228*, 15.

(12) Cong, P.; Mokhtari, A.; Zewail, A. H. *Chem. Phys. Lett.* **1990**, *172*, 109.

(13) Knopp, G.; Schmitt, M.; Materny, A.; Kiefer, W. *J. Phys. Chem. A* **1997** *101*, 4852.

(14) Lienau, C.; Zewail, A. H. *J. Phys. Chem.* **1996**, *100*, 18629.

(15) Materny, A.; Lienau, C.; Zewail, A. H. *J. Phys. Chem.* **1996**, *100*, 18650.

(16) Liu, Q.; Wan, C.; Zewail, A. H. *J. Phys. Chem.* **1996**, *100*, 18666.

(17) Blum, K. *Density Matrix Theory and Applications*, 2nd ed.; Plenum Press: New York, 1996. Mukamel, S. *Principles of Nonlinear Optical Spectroscopy*; Oxford University Press: New York, 1995.

(18) Schinke, R. *Photodissociation Dynamics*; Cambridge University Press: Cambridge, 1993.

(19) Saalfrank, P.; Kosloff, R. *J. Chem. Phys.* **1996**, *105*, 2441. Stock, G.; Thoss, M. *Phys. Rev. Lett.* **1997**, *107*, 6230. Gerdts, T.; Manthe, U. *J. Chem. Phys.* **1997**, *106*, 3017. Jungwirth, P.; Fredj, E.; Gerber, R. B. *J. Chem. Phys.* **1996**, *104*, 9332. Worth, G.; Meyer, H.-D.; Cederbaum, L. S. *J. Chem. Phys.* **1996**, *105*, 4412. Burghardt, I. *J. Chem. Phys.* Femtochemistry Special Issue, in press.

(20) Li, Z.; Zadoyan, R.; Apkarian, V. A.; and Martens, C. C. *J. Phys. Chem.* **1995**, *99*, 7453. Zadoyan, R.; Li, Z.; Martens, C. C., Apkarian, V. A. *J. Chem. Phys.* **1994**, 101, 6648. Sterling, M.; Zadoyan, R.; Apkarian, V. A. *J. Chem. Phys.* **1996**, *104*, 6497. Zadoyan, R.; Sterling, M.; Ovchinnikov, M.; Apkarian, V. A. *J. Chem. Phys.* **1997**, *107*, 8446.

(21) Whitnell, R. M.; Wilson, K. R.; Yan, Y., Zewail, A. H. *J. Mol. Liq.* **1994**, *61*, 153.

(22) Batista, V. S.; Coker, D. F. *J. Chem. Phys.* **1997**, *106*, 6923.

(23) Dietz, H.; Knopp, G.; Materny, A.; Engel, V. *Chem. Phys. Lett.* **1997**, *275*, 519.

(24) Gutzwiller, M. C. *Chaos in Classical and Quantum Mechanics*; Springer: New York, 1990.

(25) Engel, V. *Comput. Phys. Commun.* **1991**, *63*, 228.

(26) Feit, M. D.; Fleck, J. A.; Steiger, A. *J. Comput. Phys.* **1982**, *47*, 412.

(27) Bersohn, R.; Zewail, A. H. *Ber. Bunsen-Ges. Phys. Chem.* **1988**, *92*, 373. Bernstein, R. B.; Zewail, A. H. *J. Chem. Phys.* **1989**, *90*, 829.

(28) Zhiming, L.; Fang, J.-Y.; Martens, C. C. *J. Chem. Phys.* **1996**, *104*, 6919.

(29) Levine, R. D.; Bernstein, R. B. *Molecular Reaction Dynamics*; Oxford University Press: New York, 1987.

(30) Wilson, J. W.; Heinbockel, J. H.; Outlaw, R. A. *J. Chem. Phys.* **1988**, *89*, 929.

(31) Engel, V.; Metiu, H.; Almeida, R.; Marcus, R. A.; Zewail, A. H. *Chem. Phys. Lett.* **1988**, *152*, 1. Engel, V.; Metiu, H. *J. Chem. Phys.* **1989**, *90*, 6116.

(32) Mokhtari, A.; Cong, P.; Herek, J. L.; Zewail, A. H. *Nature* **1990**, *348*, 225. Cong, P.; Roberts, G.; Herek, J. L.; Mokhtari, A.; Zewail, A. H. *J. Phys. Chem.* **1996** *100*, 7832.

(33) Engel, V.; Metiu, H. *J. Chem. Phys.* **1989** *91*, 1596.

(34) Dietz, H.; Engel, V., in preparation.

(35) Lee, S.-Y. In ref 6, Chapter 7. Smith, T. J.; Ungar, L. W.; Cina, J. A. *J. Lumin.* **1994**, *58*, 66. Braun, M.; Meier, C.; Engel, V. *J. Chem. Phys.* **1995**, *103*, 7907.

(36) Yoshida, H. *Phys. Lett. A* **1990**, *150*, 262. Bandrauk, A. D.; Shen, H. *Chem. Phys. Lett.* **1991**, *176*, 428.